Engineering 5 (2019) 535–547

Contents lists available at ScienceDirect

Engineering

journal homepage: www.elsevier.com/locate/eng

Research
Engines and Fuels—Review

A High-Efficiency Two-Stroke Engine Concept: The Boosted Uniflow Scavenged Direct-Injection Gasoline (BUSDIG) Engine with Air Hybrid Operation

Xinyan Wang *, Hua Zhao

Center for Advanced Powertrain and Fuels, Brunel University London, Uxbridge UB8 3PH, UK

ARTICLE INFO

Article history:
Received 22 July 2018
Revised 2 January 2019
Accepted 18 March 2019
Available online 7 May 2019

Keywords:
Two-stroke engine
Uniflow scavenging
Engine design
Engine simulation
Scavenging performance
Thermal efficiency

ABSTRACT

A novel two-stroke boosted uniflow scavenged direct-injection gasoline (BUSDIG) engine has been proposed and designed in order to achieve aggressive engine downsizing and down-speeding for higher engine performance and efficiency. In this paper, the design and development of the BUSDIG engine are outlined discussed and the key findings are summarized to highlight the progress of the development of the proposed two-stroke BUSDIG engine. In order to maximize the scavenging performance and produce sufficient in-cylinder flow motions for the fuel/air mixing process in the two-stroke BUSDIG engine, the engine bore/stroke ratio, intake scavenge port angles, and intake plenum design were optimized by three-dimensional (3D) computational fluid dynamics (CFD) simulations. The effects of the opening profiles of the scavenge ports and exhaust valves on controlling the scavenging process were also investigated. In order to achieve optimal in-cylinder fuel stratification, the mixture-formation processes by different injection strategies were studied by using CFD simulations with a calibrated Reitz–Diwakar breakup model. Based on the optimal design of the BUSDIG engine, one-dimensional (1D) engine simulations were performed in Ricardo WAVE. The results showed that a maximum brake thermal efficiency of 47.2% can be achieved for the two-stroke BUSDIG engine with lean combustion and water injection. A peak brake toque of 379 N·m and a peak brake power density of 112 $kW \cdot L^{-1}$ were achieved at 1600 and 4000 $r \cdot min^{-1}$, respectively, in the BUSDIG engine with the stoichiometric condition.

1. Introduction

Engine downsizing and down-speeding technologies have been widely adopted to improve the efficiency of automotive engines through reduced engine size/weight, lower heat-transfer loss and friction loss, and an expanded high-efficiency region that covers more engine-operating points in the real driving cycle. However, the direct application of downsizing and down-speeding in a four-stroke engine can lead to severe abnormal combustion, such as knocking combustion [1], as well as low-speed pre-ignition [2]. In contrast, the peak in-cylinder pressure of a two-stroke engine [3,4] can be reduced at the same torque output due to the doubled firing frequency, which effectively minimizes the risk of abnormal combustion as observed in four-stroke counterparts. Efficient controlled auto-ignition (CAI) combustion [5–8] or spark-assisted CAI combustion [9,10] can easily be achieved by trapping the hot burned gas in a two-stroke engine due to the larger valve overlap. In addition, a compact two-stroke engine offers a higher power-to-weight ratio, which further improves the engine fuel economy.

In consideration of these advantages of two-stroke engines, a novel boosted uniflow scavenged direct-injection gasoline (BUSDIG) engine was designed in this research for higher power performance and better fuel economy. The impacts of the key components and parameters of the two-stroke BUSDIG engine—including the engine bore/stroke (*B*/*S*) ratio [11], scavenge port angles [12–14], opening profiles of the scavenge ports and exhaust valves [15], intake plenum [16], and injection strategies [17,18]—on the scavenging performance and charge preparation have been investigated in detail at Brunel University London, starting in 2015. The methodologies and key findings are summarized in this paper in order to highlight the progress of the development of the high-efficiency two-stroke BUSDIG engine.

* Corresponding author.
E-mail address: xinyan.wang@brunel.ac.uk (X. Wang).

https://doi.org/10.1016/j.eng.2019.03.008
2095-8099/

The concept of the proposed two-stroke BUSDIG engine is discussed in detail in Section 2, and the methodologies applied in this research are provided in Section 3. Section 4 summarizes the detailed research that was performed on the impacts of the key components and parameters of the two-stroke BUSDIG engine using computational fluid dynamics (CFD) simulations, while Section 5 explores the potential of the BUSDIG engine in terms of efficiency and power performance with one-dimensional (1D) engine simulations.

2. The concept of the two-stroke BUSDIG engine

Fig. 1 shows the schematic of the design of the two-stroke BUSDIG engine. In order to maximize the scavenging performance and minimize the charge short-circuiting phenomenon in the two-stroke engine, the uniflow scavenge method [19–23] was adopted. As shown in the figure, the intake scavenge ports are placed at the bottom of the cylinder liner, and the movement of the piston top directly controls the opening and closure of the scavenge ports. An intake plenum around the scavenge ports was designed to connect the scavenge ports with the intake boost system. A pent-roof cylinder head was designed with two exhaust valves on the right-hand side and one air-transfer valve for air hybrid operation on the left. The variable valve actuation (VVA) system can be applied to the exhaust valves to assist control of the scavenging process. The air hybrid concept [24] can be applied through the air-transfer valve to transfer the brake energy into high-pressure compressed air, which can then be used to restart the engine or compensate the boost system. During the air hybrid operation, the exhaust valves are deactivated, while the air-transfer valve is opened before top dead center (TDC) in order to collect the compressed air into a high-pressure tank and brake the engine. In addition to the exhaust valves and air-transfer valve on the cylinder head, the engine has a centrally mounted direct injector and a spark plug. Fuel short-circuiting can be completely avoided by applying the direct injection (DI) after the closure of the scavenge ports and exhaust valves. A shallow bowl piston was designed to form an optimal stratified fuel/air charge around the spark plug. The other specifications are summarized in Table 1.

The adopted uniflow scavenging method enables the application of a VVA system to the exhaust valves. As a result, flexible adjustment of the valve lift and timing of exhaust valves can be used to avoid or minimize the air short-circuiting phenomenon and maintain a stoichiometric mixture for the application of a three-way catalyst. Even for operating conditions with an air short-circuiting phenomenon, a three-way catalyst can function at acceptable efficiency for most of the exhaust process, since air short-circuiting generally occurs only at the end of scavenging [25]. In addition, the application of diluted or lean combustion through low-temperature combustion modes, such as CAI or spark-assisted CAI combustion, make it possible to realize high-efficiency and low-emission combustion in two-stroke operation [26,27]. In the worst-case scenario, a two-stroke engine can still be fitted with a well-assessed after-treatment device in order to resolve the emission issues [25].

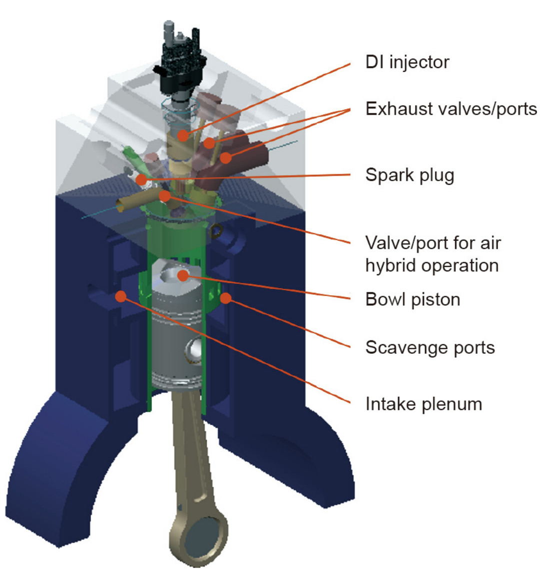

Fig. 1. Schematic of the design of the BUSDIG engine.

Table 1
Specifications of the two-stroke BUSDIG engine.

Property	Specification
Displacement	0.5 L
Compression ratio	14:1
Cylinder head	Pent-roof
	Two exhaust valves
	One air-transfer valve
	One centrally mounted injector
	One spark plug
Piston	Bowl piston
Scavenge ports	12 ports on cylinder liner

3. Methodologies

3.1. 3D CFD simulations

The three-dimensional (3D) CFD simulations were performed in STAR-CD software [28]. The Reynolds–Averaged Navier–Stokes (RANS) approach was applied in the simulations and a renormalization group (RNG) k–ε turbulence model [29] was adopted. The enthalpy conservation equation [30] was applied to calculate the heat transfer of the fluid mixture, while the Angelberger wall function [31] was adopted to calculate the wall heat transfer. For fuel-injection modeling, the droplet size was initialized with the Rosin–Rammler equations [32]; the Reitz–Diwakar breakup model [33] was then applied to model the subsequent droplet breakup process. Droplet collision was considered with the O'Rourke model [28], while droplet wall impingement was modeled with Bai model [34].

Moving mesh was applied in the simulations, and an arbitrary sliding interface (ASI) was applied to control the connectivity between the scavenge port domains and the cylinder domain with the piston movement, as well as the connectivity between the exhaust domains and the cylinder domain with the movement of the exhaust valves. An average grid size of 1.6 mm was applied for the moving mesh based on a mesh-sensitivity study [12].

The time-step was fixed at 0.1 crank angle degree (°CA) for the simulations without fuel injection and reduced to 0.05 °CA for the cases with fuel injection. The pressure-implicit with splitting of operators (PISO) algorithm [35] was applied to solve the Navier–Stokes equations. The 1D engine simulations, as detailed in next section, were used to provide realistic initial and boundary conditions for the CFD simulations.

3.2. 1D engine simulations

In order to evaluate the potential of the two-stroke BUSDIG engine in terms of efficiency and power performance, 1D engine simulations of a two-cylinder 1 L BUSDIG engine were performed in Ricardo WAVE software based on the optimal design. Fig. 2

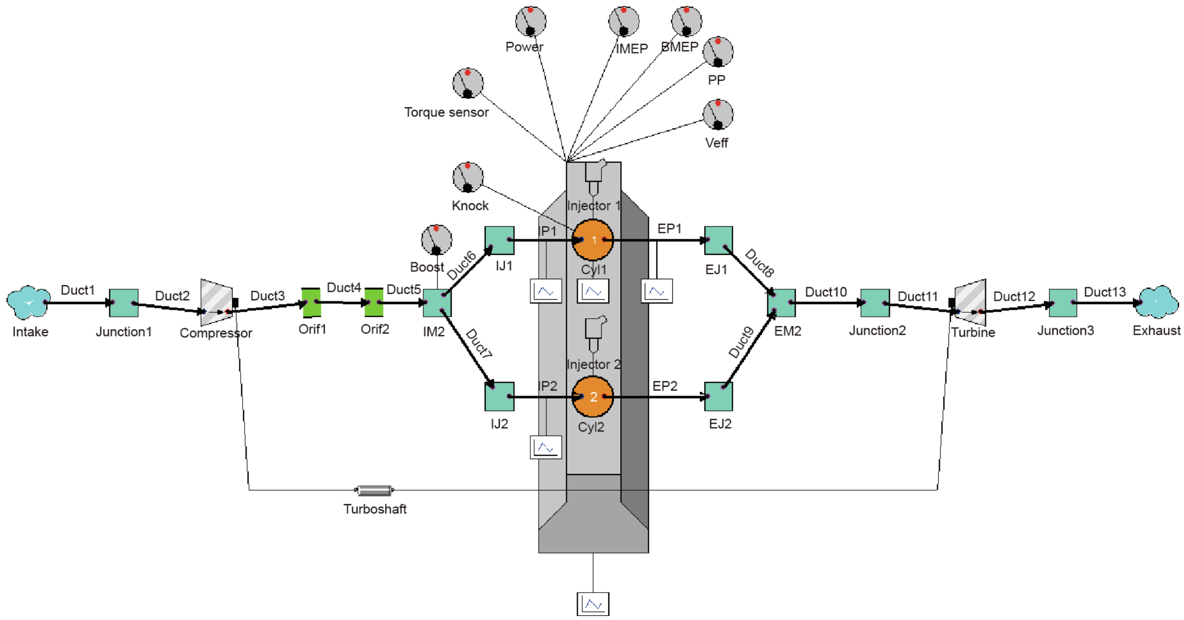

Fig. 2. 1D engine simulation model of the BUSDIG engine in Ricardo WAVE. IMEP: mean effective pressure; BMEP: brake mean effective pressure; PP: peak pressure; Veff: voltage effective value; Orif: orifice; IM: intake manifold; IJ: intake junction; IP: intake port; EP: exhaust port; EJ: exhaust junction; EM: exhaust manifold; Cyl: cylinder.

shows the schematic of the 1D simulation model of the BUSDIG engine. The flow coefficients for the intake scavenge ports and exhaust valves in the 1D engine model were calibrated against the corresponding mass flow rates obtained from 3D CFD simulation. The scavenging curve, which was used to calculate the in-cylinder exhaust gas fraction during the scavenging process, was also calibrated by CFD simulation results. The direct-injection timing was fixed at 90 °CA before TDC.

The spark ignition (SI) Wiebe heat-release model was applied to calculate the combustion process in the BUSDIG engine. The SI Wiebe function has been widely used to describe the fuel burning rate in SI engines; it allows the independent input of function shape parameters and of combustion duration. The impact of the flow motions and fuel stratification on the heat-release process was not considered. The combustion phasing (crank angle at 50% burned mass) and combustion duration (10%–90% of burned mass) were swept to determine the optimal combustion performance of the BUSDIG engine at each operating point. In order to consider the knocking combustion, the knock intensity normalized as a fraction of the fuel remaining at the time of the knock event was predicted with a knock sub-model [36] and controlled below 0.1 for each operating point. The in-cylinder peak pressure (PP) and peak pressure rise rate (PPRR) were controlled under 1.6×10^4 kPa and 1000 kPa·°CA^{-1}.

In order to predict friction loss in the BUSDIG engine, the Chen–Flynn friction model [37] was applied and calibrated with the experimental friction data [38]. A turbocharger system with the "mapless" approach [39,40] was included in the engine model to provide sufficient fresh intake air to the BUSDIG engine.

4. Design and optimization of the BUSDIG engine

The scavenging process is essential for a two-stroke engine due to its relatively longer overlap between the intake and exhaust process, which can lead to the short-circuiting phenomenon [41]. Compared with the conventional loopflow and crossflow scavenging methods, uniflow scavenging has been shown to have a superior scavenging performance, as evidenced by both optical measurements [42,43] and numerical simulations [19–23]. The impacts of several key design parameters of the BUSDIG engine—including the engine *B/S* ratio, scavenge port angles, intake plenum and opening profiles of the scavenge ports and exhaust valves, and direct-injection strategies—on the scavenging process, in-cylinder flow motion, and subsequent fuel/air mixing process are discussed in this section.

The main objective of the optimization of the scavenging performance is to achieve a higher charging efficiency (CE) and scavenging efficiency (SE) with fixed boost pressure. CE can be calculated by multiplying the delivery ratio (DR) and trapping efficiency (TE), and directly determines how much intake fresh charge can be retained in the cylinder for the subsequent combustion process. Therefore, increasing either the DR or TE increases the CE. A higher CE is especially crucial for high-speed high-load operating conditions, which demand more fresh charge to meet the load requirement. Meanwhile, the SE determines how much hot residual gas will be retained in the cylinder relative to the total retained charge. Considering the potential impact of the hot residual gas on the knocking combustion, a higher SE is desirable in order to minimize the knocking tendency.

Strong in-cylinder flow motions can enhance the mixing process of the directly injected fuel and in-cylinder mixture [44], which is important for a two-stroke engine with late injection timings. However, given the increased heat-transfer loss due to flow motions [45], moderate swirl and tumble ratios are preferable in order to balance their impact on enhancing fuel/air mixing and heat-transfer loss for the BUSDIG engine.

4.1. Bore/stroke ratio

The *B/S* ratio affects both engine performance and overall dimension for a fixed engine displacement. A small *B/S* ratio tends to result in higher engine efficiency, while a larger *B/S* ratio produces higher power density [46]. Regarding the exhaust emissions, the design with an increased crevice volume and a larger *B/S* ratio produced higher carbon monoxide (CO) and hydrocarbon (HC) emissions [47,48] but lower nitrogen oxides (NO_x) emissions [47]. Most importantly, the engine performances are more affected by the *B/S* ratio for a two-stroke engine than a four-stroke counterpart due to the direct impact of the *B/S* ratio on the scavenging process in a two-stroke engine [49–52].

Therefore, in order to understand the impact of the design of the *B/S* ratio on the scavenging process, different bore and stroke values were designed with a *B/S* ratio ranging from 0.66 to 1.3, as shown in Table 2 [11]. The connecting rod was fixed at 180 mm for all the designs. Fig. 3 shows the schematic diagram of the adopted engine design described in this section. Initially, a simplified engine design with two groups of scavenge ports on the two sides of the cylinder was applied to study the impact of *B/S* ratio. The width of each scavenge port was kept constant at 20° for all *B/S* ratio designs. The interval between adjacent scavenge ports in each group was fixed at 10°, while the interval between the two groups was set at 70°. The axis inclination angle (AIA) and swirl orientation angle (SOA) of the scavenge ports were fixed at 90° and 20°, respectively. More information on the impact of the scavenge port angles on the scavenging process with different *B/S* ratios can be found in Ref. [11]. The scavenge port height was fixed at 14 mm and the scavenge port opening timing was set to 122 °CA. The intake boost pressure was fixed at 200 kPa, and engine speed was set to 2000 r·min^{-1} for all cases. The exhaust valve duration (ED) and exhaust valve opening timing (EVO) were fixed at 126 and 117 °CA, respectively.

The swirl ratio (SR), tumble ratio (TR), and cross-tumble ratio (CTR) [53] after the scavenging were calculated in order to quantify the flow motions in the BUSDIG engine for different *B/S* ratios; the results are shown in Fig. 4. Overall, the in-cylinder flow motion in the BUSDIG engine was characterized with strong swirl flow but very weak tumble and cross-tumble flows. The increase of the *B/S* ratio slightly decreased the SR but had less impact on the TR and CTR. The decreased SR can be attributed to a larger bore design and less momentum being transferred to the in-cylinder charge due to an enhanced charge short-circuiting process with a larger *B/S* ratio design [11].

Four scavenging parameters—namely, the DR, TE, SE, and CE [12]—were used to characterize the engine scavenging performance; the corresponding results are shown in Fig. 5. As the *B/S* ratio increased, the engine was characterized by a larger bore but a shorter stroke, leading to a significantly enhanced short-circuiting phenomenon due to the shorter distance between the intake scavenge ports and the exhaust valves [11]. As a result, the DR showed an increasing trend with the *B/S* ratio, as shown in Fig. 5, due to lower scavenging resistance with the stronger short-circuiting phenomenon. However, the *B/S* ratio had less impact on the SE and CE. As a result, the TE was gradually reduced with the *B/S* ratio. Overall, a higher *B/S* ratio tended to increase the DR, which in turn led to a slightly higher SE. The largest *B/S* ratio of 1.3 produced the highest CE but the lowest TE.

Table 2
Design of the *B/S* ratio.

No.	Bore (mm)	Stroke (mm)	*B/S* ratio
1	75	113	0.66
2	80	100	0.80
3	86	86	1.00
4	94	72	1.30

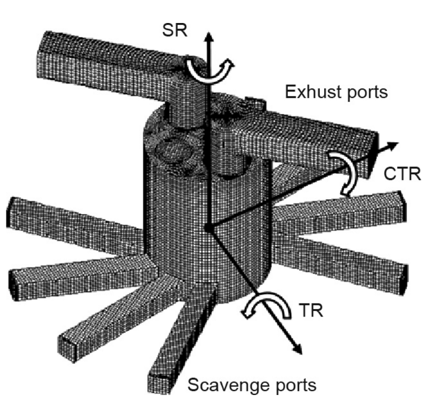

Fig. 3. Schematic diagram of the engine design for the *B/S* ratio study. Reproduced from Ref. [11] with permission of Institution of Mechanical Engineers, © 2018.

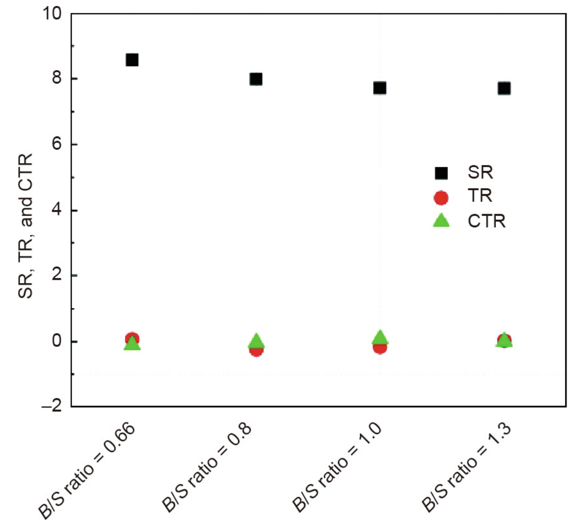

Fig. 4. SR, TR, and CTR at 280 °CA with different *B/S* ratios. Reproduced from Ref. [11] with permission of Institution of Mechanical Engineers, © 2018.

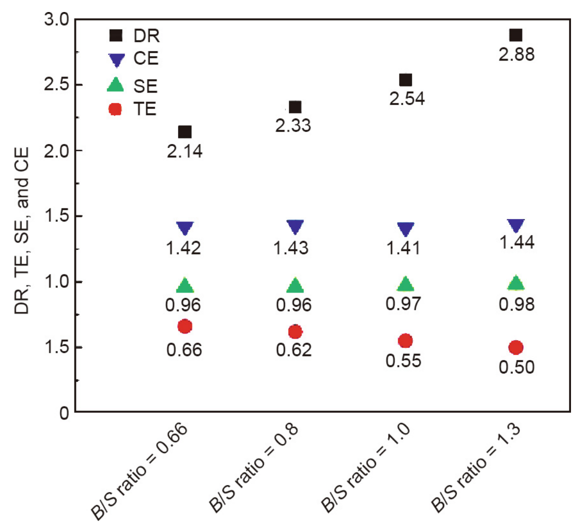

Fig. 5. Effect of *B/S* ratio on DR, TE, SE, and CE. Reproduced from Ref. [11] with permission of Institution of Mechanical Engineers, © 2018.

Considering the relatively better performance in CE and TE and the moderate in-cylinder flow motions for the subsequent fuel/air mixing process, a *B/S* ratio of 0.8 with a bore of 80 mm and a stroke of 100 mm was finally selected as the optimal design and applied for the subsequent study.

4.2. Scavenge port angles

Like the engine *B/S* ratio, the intake scavenge port design directly affects the scavenging process in two-stroke engines. Uniflow scavenged two-stroke engines are characterized by a strong swirl flow motion formed by the angled intake scavenge ports at the bottom of the cylinder liner [43,54,55]; furthermore, the SOA

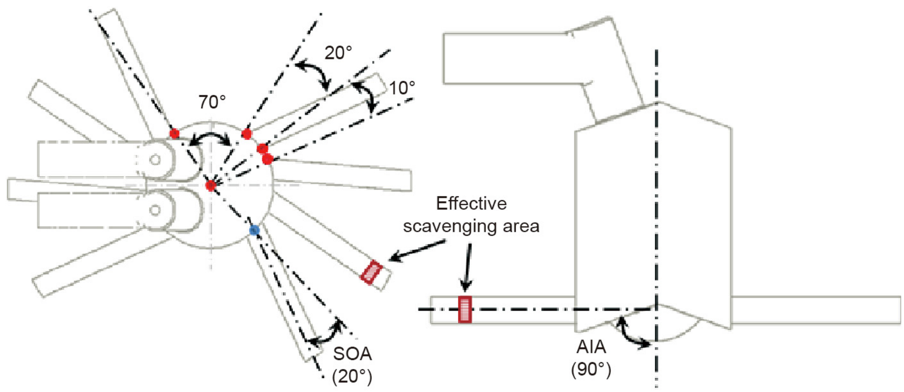

Fig. 6. Definition of the scavenge port angles. Reproduced from Ref. [13] with permission of Institution of Mechanical Engineers, © 2018.

and AIA of the scavenge ports have the greatest impact on the in-cylinder flow motions and scavenging performances [22,23,56].

Therefore, the AIA and SOA were investigated in order to optimize the in-cylinder flow motions and maximize the scavenging performance of the BUSDIG engine. (Definitions of AIA and SOA are illustrated in Fig. 6.) An optimal *B/S* ratio of 0.8 was applied in this part of the research. The other setups, including the opening timing of the scavenge ports and exhaust ports, engine speed, and intake boost pressure, were kept the same as described in Section 4.1.

The AIA was varied between 60° and 90° in order to investigate its impact on the scavenging process, while the SOA was fixed at 20°. As shown in Fig. 7, the in-cylinder swirl flow motion was very strong regardless of the AIA. The maximum SR was achieved at the largest AIA (90°). In comparison, the maximum TR and CTR were achieved at an intermediate AIA (68°–75°).

Fig. 8 shows the impact of the AIA on the scavenging performances. The DR showed an increasing trend with the AIA due to an increased effective scavenging area. In addition, a larger AIA tended to minimize the charge short-circuiting and thereby improve the CE. However, it was found that the AIA had little impact on the SE and TE.

As the flow motions were comparable for different AIAs, a higher scavenging performance was preferable in order to achieve an overall improvement in the engine performance. Therefore, an AIA of 90° was selected as the optimal value for the BUSDIG engine.

The impact of the SOA on the in-cylinder flow motions and scavenging performances was investigated by adjusting the SOA from 0 to 31.5°. The AIA was fixed at the optimal value of 90°.

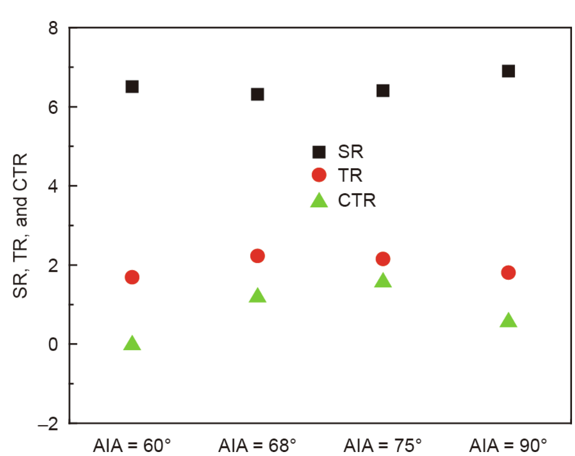

Fig. 7. SR, TR, and CTR with different AIAs, SD = 116 °CA, ED = 126 °CA, EVO = 117 °CA. Reproduced from Ref. [13] with permission of Institution of Mechanical Engineers, © 2018.

The increase of the SOA significantly enhanced the in-cylinder swirl flow motion due to the effective guidance on the intake flow around the swirl axis by the angled scavenge ports. This was evidenced by the almost linear correlation between the SOA and SR,

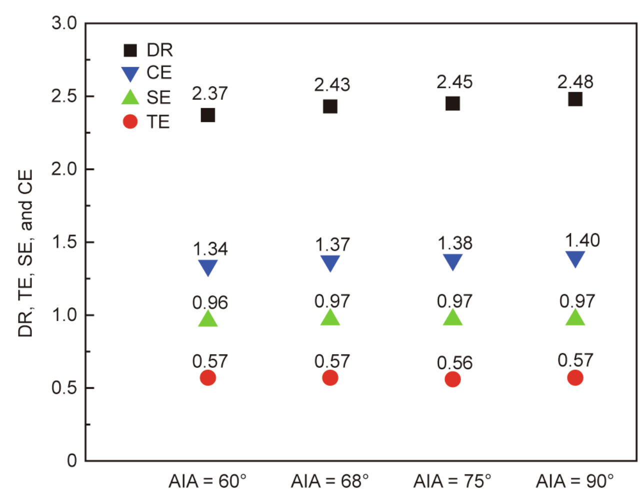

Fig. 8. DR, TE, SE, and CE with different AIAs. SD = 116 °CA, ED = 126 °CA, EVO = 117 °CA. Reproduced from Ref. [13] with permission of Institution of Mechanical Engineers, © 2018.

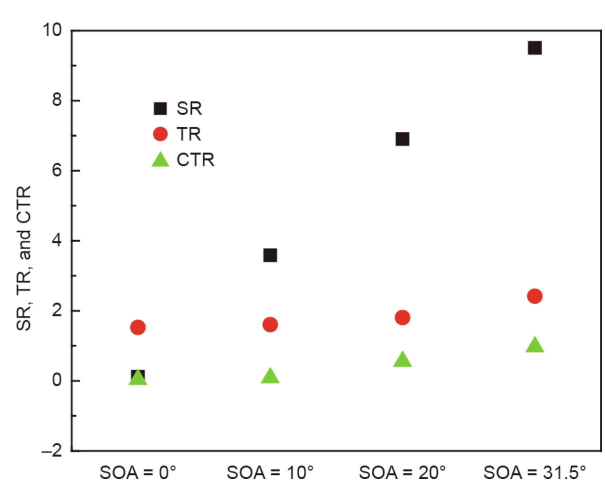

Fig. 9. SR, TR, and CTR at 280° with different SOAs, SD = 116 °CA, ED = 126 °CA, EVO = 117 °CA. Reproduced from Ref. [13] with permission of Institution of Mechanical Engineers, © 2018.

as shown in Fig. 9. Meanwhile, the TR and CTR also showed a slightly increasing trend with the SOA.

The scavenging performance with different SOAs is shown in Fig. 10. An increase in the SOA reduced the effective scavenging area of the scavenge ports, which gradually decreased the DR. The maximum CE was achieved with a SOA of 20°. A smaller SOA led to strong collision of the intake air jets in the cylinder center and resulted in stronger short-circuiting [13], thus producing a lower CE. In contrast, a greater SOA led to a reduced DR and early short-circuiting near the cylinder wall due to the stronger swirl flow motion [13]; this in turn lowered the CE and SE [13]. The TE showed a slightly increasing trend with the SOA, as the DR was reduced more significantly than the CE. Overall, a SOA of 20° was found to be optimal and was applied for the subsequent study, as it provided the highest CE along with moderate in-cylinder flow motions.

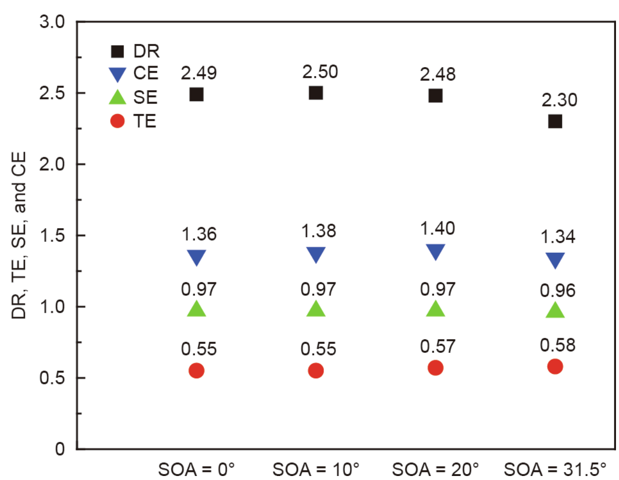

Fig. 10. DR, TE, SE, and CE with different SOAs, SD = 116 °CA, ED = 126 °CA, EVO = 117 °CA. Reproduced from Ref. [13] with permission of Institution of Mechanical Engineers, © 2018.

4.3. Design of the intake plenum

The intake plenum of the BUSDIG engine was designed to accommodate the scavenge ports and connect them to the intake boost system in order to provide sufficient intake charge. The design of the intake plenum of a uniflow engine has been shown to have an impact on both the in-cylinder flow motions and the scavenging performances [22,23,57–59]. It was found that application of an intake plenum could produce a non-identical and skewed scavenging flow [23], and that a larger intake plenum volume provided a constant pressure for the scavenging process [57]. Therefore, several key design parameters of the intake plenum were investigated by 3D CFD simulations [16] in order to achieve sufficient in-cylinder flow motions and better scavenging performances in the BUSDIG engine. In this study, 12 evenly distributed scavenge ports were applied, with the width of each scavenge port set as 20° and the interval between two adjacent scavenge ports set as 10°. The AIA and SOA of the scavenge ports were fixed at 90° and 20°, respectively. The other setups, including the opening timing of the scavenge ports and exhaust ports and the boost pressure, were kept the same as described in Section 4.1.

Fig. 11 shows the design of the intake plenum with an inlet pipe and a scavenge chamber. Five important design parameters of the intake plenum were identified and investigated with CFD simulations in order to optimize the in-cylinder flow motions and scavenging performances in the BUSDIG engine.

The first design parameter was defined as the ratio of the inlet area relative to the scavenge port area ($r_{I/S}$). Figs. 12 and 13 show the effect of $r_{I/S}$ on the in-cylinder flow motions and scavenging performances at 2000 r·min^{-1}. It should be noted that $r_{I/S}$ was adjusted from 0.68 to 1.36 by increasing the inlet pipe height from 20 to 40 mm with a fixed inlet pipe width. Overall, the SR was slightly reduced with the increase of $r_{I/S}$. The tumble and cross-tumble flows tended to transfer to each other due to the interaction with the strong swirl flow during scavenging, and showed reversed trends with $r_{I/S}$. This tradeoff relationship between the TR and CTR was a typical phenomenon that was also observed for other designs. Regarding the scavenging performance, the plenum design with the largest $r_{I/S}$ (i.e., 1.36) produced the highest DR

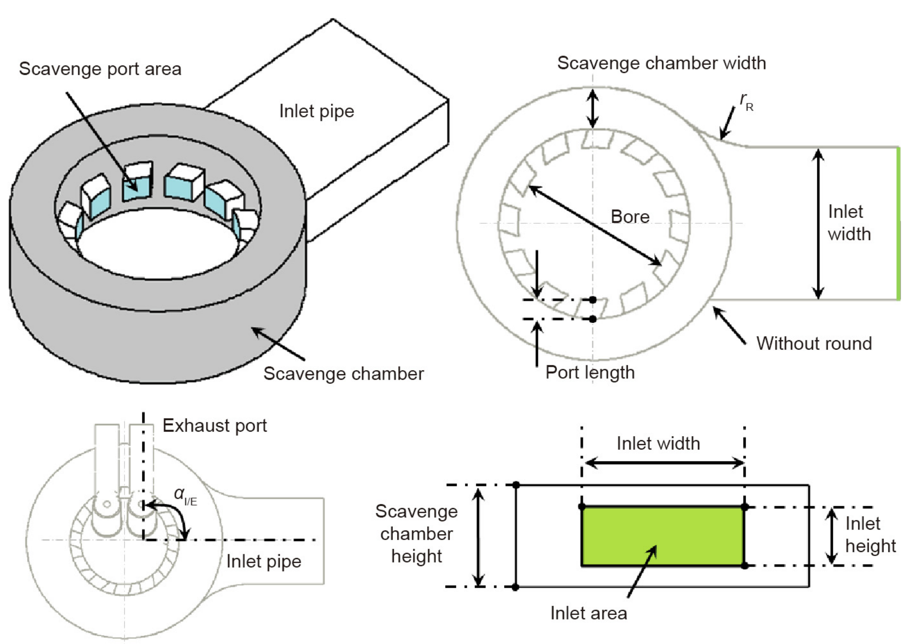

Fig. 11. Schematic of the design of the intake plenum. Reproduced from Ref. [16] with permission of SAE International, © 2017.

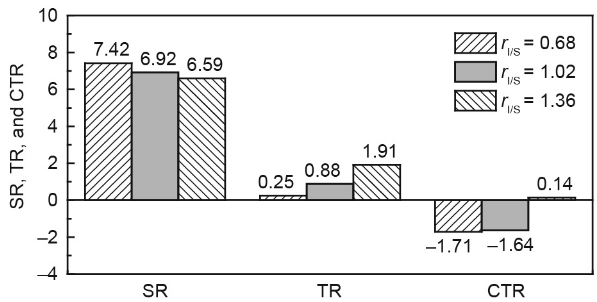

Fig. 12. Effect of $r_{I/S}$ on SR, TR, and CTR at 280 °CA. Reproduced from Ref. [16] with permission of SAE International, © 2017.

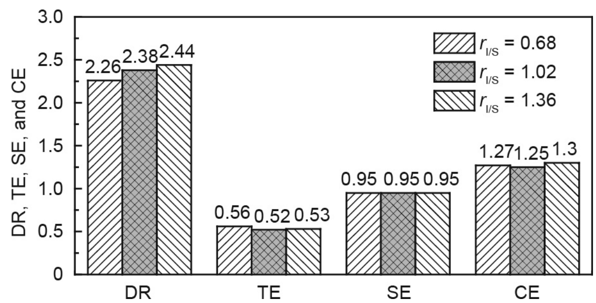

Fig. 13. Effect of $r_{I/S}$ on DR, TE, SE, and CE. Reproduced from Ref. [16] with permission of SAE International, © 2017.

and CE, as shown in Fig. 13. The SE was not affected by $r_{I/S}$ and was fixed at 0.95 for each design. Overall, a larger $r_{I/S}$ resulted in better scavenging performance with sufficient in-cylinder flow motions.

The radius of the round connecting the inlet pipe and the scavenge chamber (r_R) showed very limited impact on the in-cylinder flow motions and scavenging performances [16]. Therefore, the results are not shown here for simplicity.

The ratio of the scavenge chamber volume to the cylinder displacement volume ($r_{S/C}$) was varied from 0.84 to 3.02 by increasing the scavenge chamber width from 22 to 60 mm with a constant scavenge chamber height. Overall, the scavenge chamber volume showed a slight impact on the in-cylinder flow motions at 2000 $r{\cdot}min^{-1}$ [16]. Fig. 14 shows the scavenging performances with different $r_{S/C}$. It was found that the DR and SE monotonously increased with $r_{S/C}$ and the CE significantly increased from 1.25 to 1.41 when the $r_{S/C}$ increased from 0.84 to 1.76. Therefore, a larger scavenge chamber volume was preferable to achieve better scavenge performances in the BUSDIG engine.

The angle between the inlet pipe and exhaust pipe ($\alpha_{I/E}$) was defined to demonstrate the relative orientation between the inlet and exhaust pipes. Fig. 15 shows the impact of $\alpha_{I/E}$ on the SR, TR, and CTR. The SR decreased significantly from 6.59 to 5.08 when $\alpha_{I/E}$ was reduced from 180° to 0°. As shown in Fig. 15, vertical placement with an $\alpha_{I/E}$ of 90° was very effective in promoting the formation of tumble and cross-tumble flows. The orientation of the inlet pipe showed limited impact on the scavenging performances at 2000 $r{\cdot}min^{-1}$. Overall, the placement of the inlet and exhaust pipes on the same side ($\alpha_{I/E} = 0°$) produced a slightly higher DR than the vertical placement ($\alpha_{I/E} = 90°$), while the $\alpha_{I/E}$ had little effect on the SE and CE [16].

The ratio of the bore to scavenge port length ($r_{B/PL}$) was reduced from 16 to 4 by increasing the scavenge port length from 5 to 20 mm. Fig. 16 compares the in-cylinder flow motions with different $r_{B/PL}$. It was found that the reduction of $r_{B/PL}$ from 16 to 4 led to a significantly higher SR due to better guidance of the intake flow with longer scavenge ports. However, $r_{B/PL}$ had only a slight impact on the scavenging performance [16]. Therefore, a minimum port length of 10 mm was required to produce sufficient in-cylinder swirl flow motion for good fuel/air mixing in the BUSDIG engine.

4.4. Impact of the opening profiles of the scavenge ports and exhaust valves

As the exhaust valves are placed on the cylinder head in a uniflow scavenged two-stroke engine, the VVA system can be applied to adjust the exhaust valve lift/phasing and optimize the scavenging process. The VVA system has been demonstrated to be effective in controlling the amount of residual gases and the combustion process in two-stroke engines [60,61]. The opening timing of the scavenge ports has also been shown to have a significant impact on the scavenging performance and fuel consumption [62,63]. Therefore, as discussed in this section, a scavenging process with different opening profiles of the scavenge ports and exhaust valves was analyzed in order to clarify their impacts on the scavenging process in the BUSDIG engine [13]. Fig. 17 shows the profiles of

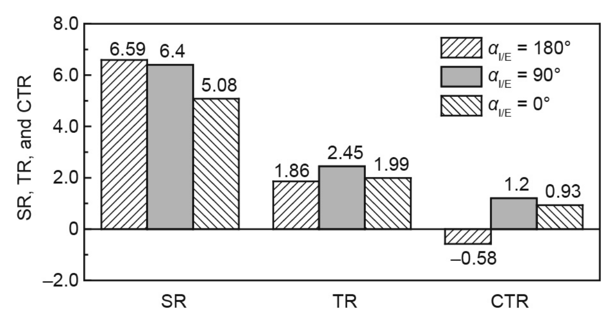

Fig. 15. Effect of $r_{I/E}$ on SR, TR, and CTR at 280 °CA. Reproduced from Ref. [16] with permission of SAE International, © 2017.

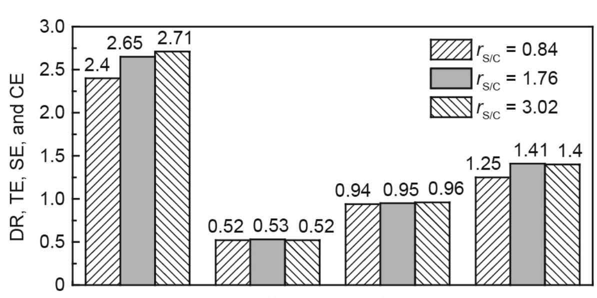

Fig. 14. Effect of $r_{S/C}$ on DR, TE, SE, and CE. Reproduced from Ref. [16] with permission of SAE International, © 2017.

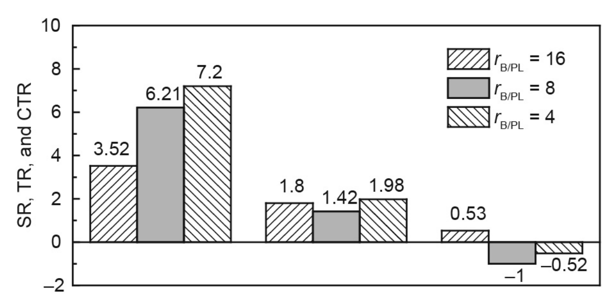

Fig. 16. Effect of $r_{B/PL}$ on in-cylinder SR, TR, and CTR at 280 °CA. Reproduced from Ref. [16] with permission of SAE International, © 2017.

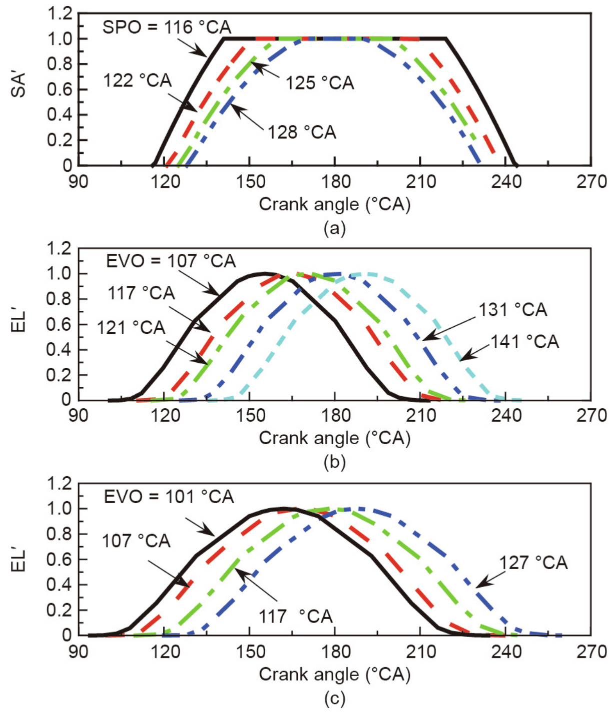

Fig. 17. Opening profiles of (a) scavenge ports and exhaust valves with ED of (b) 98 °CA and (c) 126 °CA. Reproduced from Ref. [13] with permission of Institution of Mechanical Engineers, © 2018.

the normalized scavenge port opening area (SA′) and the exhaust valve lift (EL′) used in this part of the research. As shown in the figure, the scavenge port opening (SPO) timing was varied from 116 to 128 °CA. The opening duration of the scavenge ports (SD) was correspondingly decreased from 128 to 104 °CA. Regarding the opening profiles of exhaust valves, two opening durations (ED) were applied in this study. For the short duration design with an ED of 98 °CA, the EVO was gradually delayed from 101 to 141 °CA. Similarly, the EVO timing was delayed from 101 to 127 °CA for the long-duration design with an ED of 126 °CA. The scavenge port angles were fixed at optimal values (AIA = 90°, SOA = 20°) for all the cases described in this section.

In order to characterize the relationships between the opening profiles of the scavenge ports and exhaust valves for the subsequent analysis of their impacts on the scavenging process, three parameters—namely, Δ_{open}, Δ_{close}, and $\Delta_{overlap}$—were defined with the following equations and are illustrated in Fig. 18.

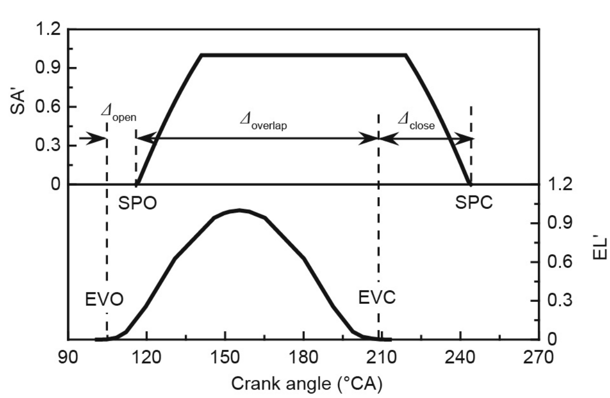

Fig. 18. Definitions of Δ_{open}, Δ_{close}, and $\Delta_{overlap}$. Reproduced from Ref. [13] with permission of Institution of Mechanical Engineers, © 2018.

$$\Delta_{open} = \mathrm{SPO} - \mathrm{EVO} \tag{1}$$

$$\Delta_{close} = \mathrm{SPC} - \mathrm{EVC} \tag{2}$$

$$\Delta_{overlap} = \min(\mathrm{SPC}, \mathrm{EVC}) - \max(\mathrm{SPO}, \mathrm{EVO}) \tag{3}$$

where SPO and SPC refer to scavenge port opening and closing, respectively; EVO and EVC refer to exhaust valve opening and closing, respectively,

Fig. 19 shows the mass flow rates and residual gas fraction (RGF) profiles at the outlets of the scavenge ports. Four scavenging periods—that is, early backflow (EB), backflow scavenging (BS), main scavenging (MS), and post backflow (PB)—were identified and are shown in Fig. 19 to demonstrate the typical scavenging process in the BUSDIG engine. At the first EB stage, the in-cylinder burned gas can be pushed back to the scavenge ports due to the relatively higher in-cylinder pressure just after the SPO. When the pressure between the intake and cylinder is balanced due to the drop of in-cylinder pressure, the second BS stage begins, with the mixture of burned gas and fresh charge in the scavenge ports entering the cylinder and scavenging out in-cylinder burned gas. At the third MS stage, the pure fresh charge (without burned gas from EB) begins scavenging the engine cylinder. In addition, the in-cylinder mixture can flow back into the scavenge ports during the compression stroke when the SPC timing is later than the EVC timing; this is defined as the PB stage.

A systematic correlation study was performed in order to understand the impact of the opening profiles of the scavenge ports and exhaust valves on the scavenging process, and the final scavenge performances based on the CFD simulation results. As an example, Fig. 20 shows negative correlations between EB duration (d_{EB}) and Δ_{open}. Similarly, a detailed correlation study was performed for other characteristic parameters [13]. The results are provided in Fig. 21, which shows that a larger Δ_{open} can be applied to maximize the SE. For the cases with PB, a larger Δ_{close} with a later SPC timing than EVC timing will decrease the CE. However, the opposite trend was found for the cases without PB. An increase of $\Delta_{overlap}$ can effectively improve the DR, which in turn improves both the SE and CE for the cases without PB. In contrast, a larger $\Delta_{overlap}$ was found to decrease the DR for the cases with PB. Therefore, the scavenging performance of the BUSDIG engine can be maximized by adjusting the parameters Δ_{close} and $\Delta_{overlap}$ to just avoid the PB. Regarding the in-cylinder flow motions, it was found

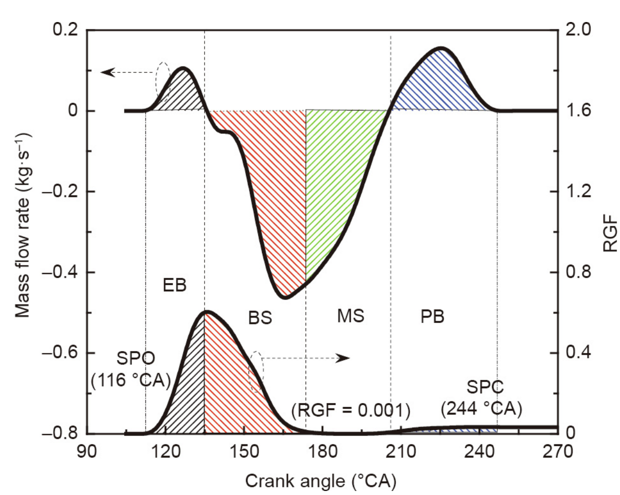

Fig. 19. Definitions of the EB, BS, MS, and PB stages based on the total mass flow rates and RGF profiles at the outlets of the scavenge ports. Reproduced from Ref. [13] with permission of Institution of Mechanical Engineers, © 2018.

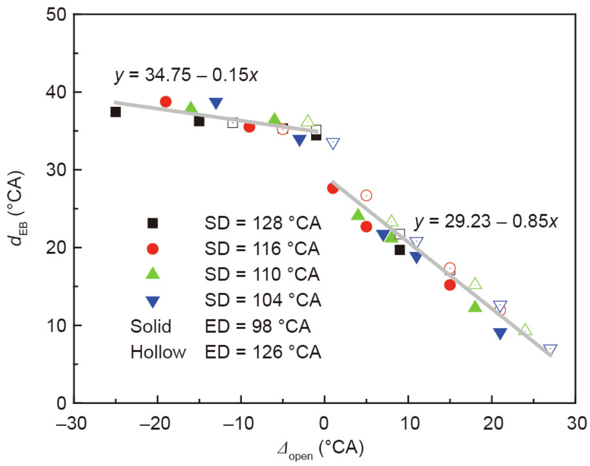

Fig. 20. Effect of Δ_{open} on d_{EB}. Reproduced from Ref. [13] with permission of Institution of Mechanical Engineers, © 2018.

that the parameter Δ_{close} showed a positive correlation with the SR but a negative correlation with the TR.

In order to completely avoid the short-circuiting phenomenon in the BUSDIG engine, a low exhaust valve lift (3 mm) was also investigated [15]. The adopted profiles of the exhaust valves and normalized scavenge port area are shown in Fig. 22.

The impact of the EVO timing of the low-lift exhaust valves on the scavenging performance is shown in Fig. 23. As no short-circuiting was found for any of the EVO timings, the TE was maintained at 1 and the CE was kept the same as the DR for all cases. It was noted that both the DR/CE and the SE gradually decreased when the EVO timing was postponed from 84 to 104 °CA. This finding was mainly attributed to the shortened blowdown duration by postponing the EVO timing. However, further delay of the EVO timing to 124 °CA directly increased the overlap between the intake and exhaust process, resulting in a slightly higher DR/CE and SE. Therefore, these results indicated that in-cylinder burned gas fraction can be adjusted by controlling the EVO timing of the exhaust valves. Avoidance of the short-circuiting phenomenon and capability of controlling in-cylinder burned gas fraction made it possible for conventional port fuel injection and gasoline compression ignition combustion to be applied in the BUSDIG engine by trapping hot burned gas [15].

Regarding the in-cylinder flow motion, the earliest EVO timing of 84 °CA produced a stronger swirl flow motion due to the longest blowdown duration. As the EVO timing was delayed from 94 to 124 °CA, the peak SR showed a decreasing trend; however, the SR at TDC was very similar among the cases. The in-cylinder tumble and cross-tumble flow motions with a low exhaust valve lift design were very weak for all EVO timings [15].

4.5. Optimization of in-cylinder mixture formation

In addition to the optimization of the scavenging process in the BUSDIG engine, the in-cylinder fuel/air mixture-preparation process required attention in order to produce a stoichiometric mixture in the vicinity of the spark plug for stable ignition kernel formation and faster flame propagation [64–67]. It was found that both injection timing [68–71] and a split ratio of multiple injections [64,68,72] showed significant impacts on in-cylinder fuel distribution and subsequent combustion.

In this research, an outward-opening piezoelectric injector was adopted in the BUSDIG engine to improve both the fuel economy and exhaust emissions due to its unique features, which include a stable recirculation pattern, shorter penetration, a precise and flexible fuel-injection rate and duration, and rapid opening and closing for multiple injections [73]. In order to understand the in-cylinder fuel injection and mixture formation in the BUSDIG engine, calibration of the breakup model was first performed with optical measurements in a constant-volume vessel at different back pressures [17]. Next, the calibrated breakup model was applied in order to understand the in-cylinder fuel injection and mixture formation process in the BUSDIG engine with various injection timings and injection strategies [18].

Both the Kelvin–Helmholtz Rayleigh–Taylor (KHRT) and Reitz–Diwakar breakup models were applied and calibrated by the corresponding measurements with an injection pressure of 1.8×10^4 kPa and backpressures of 100 and 1000 kPa, respectively. The results indicated that the calibrated Reitz–Diwakar model at a backpressure of 100 kPa was able to accurately model the gasoline sprays at a backpressure of 1000 kPa without further tuning being

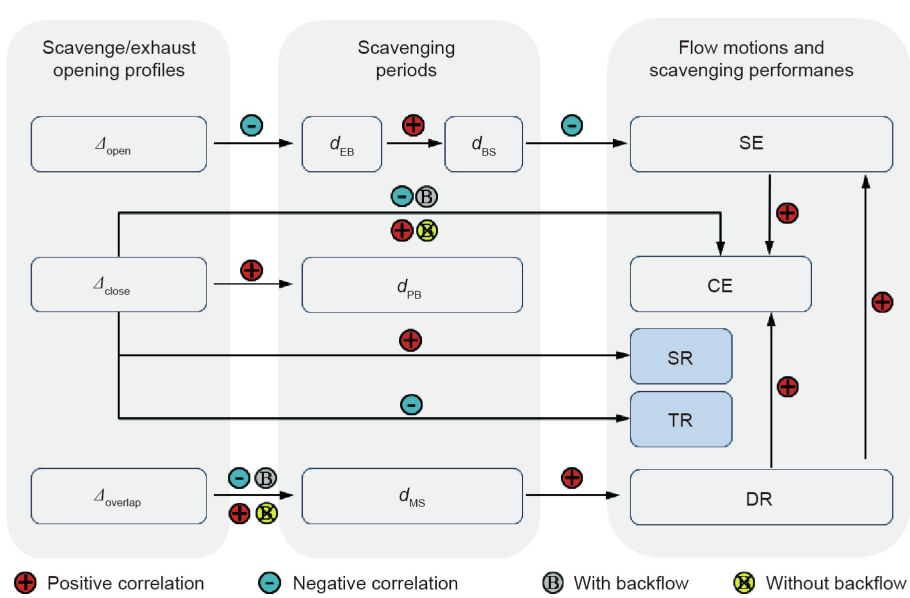

Fig. 21. Relationships among the opening profiles of scavenge ports and exhaust valves, scavenging periods, in-cylinder flow motions, and scavenging performances. Reproduced from Ref. [13] with permission of Institution of Mechanical Engineers, © 2018.

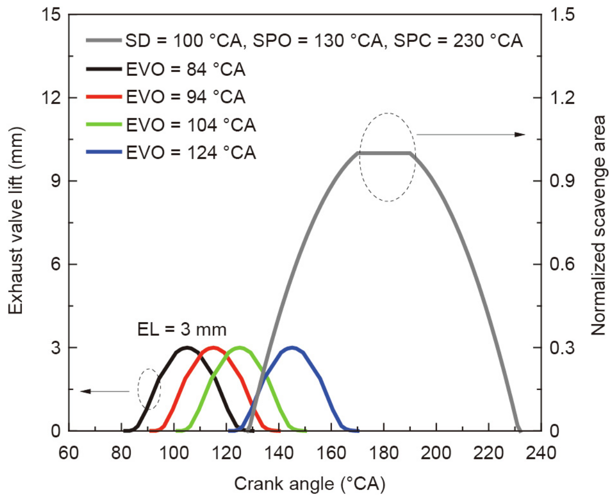

Fig. 22. The opening profiles of the low-lift exhaust valves and normalized scavenge port area. Reproduced from Ref. [15] with permission of Brunel University, © 2017.

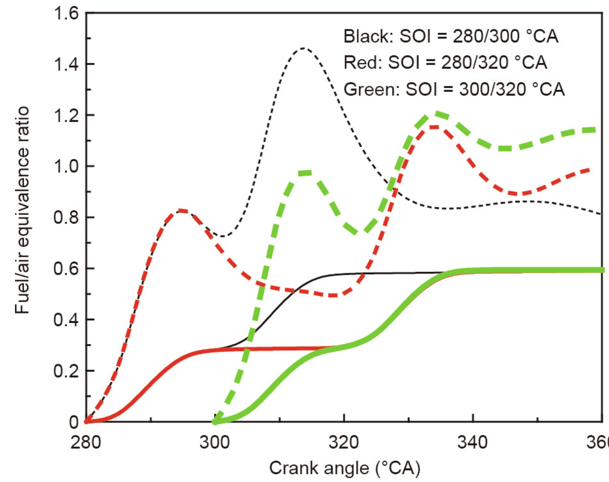

Fig. 24. Impact of start of injection (SOI) timings on the average fuel/air equivalence ratio in the whole cylinder (solid lines) and spark zone (dashed lines). Reproduced from Ref. [18] with permission of Institution of Mechanical Engineers, © 2018.

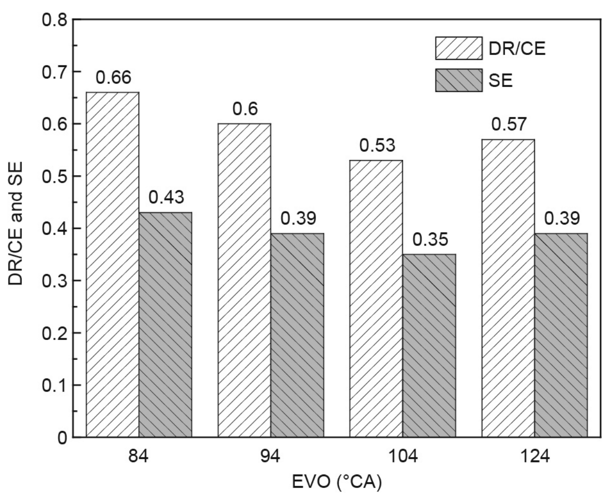

Fig. 23. Impact of EVO timing on DR/CE and SE (TE = 1 for all cases). Reproduced from Ref. [15] with permission of Brunel University, © 2017.

required [17]. Therefore, the calibrated Reitz–Diwakar breakup model was applied in subsequent engine simulations with DIs.

Fig. 24 compares the average fuel/air equivalence ratio in the whole engine cylinder and spark zone with the split-injection strategy (split ratio = 0.5) under an overall lean condition (lambda ≈ 1.7). The split ratio was defined as the ratio of the fuel mass in the first injection to the total fuel mass. A sphere with a diameter of 20 mm around the spark plug was defined as the spark zone in order to describe the fuel stratification around the spark plug. As shown in Fig. 24, the split-injection strategy with a split ratio of 0.5 produced the optimal fuel stratification with a slightly rich mixture in the spark zone and an overall lean mixture in the whole cylinder. The split injection reduced the penetration of each injection due to the lower fueling mass and positioned the recirculation region around the spark plug, which in turn enriched the mixture in the spark zone after each injection. However, it was noted that the split injection with the first injection at 280 °CA was unable to effectively stabilize the rich mixture around the spark plug before TDC, although the delay of the second injection to 320 °CA slightly enriched the mixture of the spark zone around TDC. By postponing the split injections to 300/320 °CA, a slightly rich mixture in the spark zone with a fuel/air equivalence ratio of around 1.1 can be stabilized around TDC, even under an overall lean condition (lambda ≈ 1.7).

Fig. 25 shows the distributions of the fuel/air equivalence ratio in order to clarify the mixture-preparation process in the BUSDIG engine with the split-injection strategy. The rich mixture produced by the first injection was affected strongly by the in-cylinder flow motions and was transported to the left side at 300 °CA, as shown in Section A-A of Fig. 25. On the other hand, the first injection itself also interacted with the in-cylinder flows and smoothed the flow motions in the cylinder center after the injection [18]. Therefore, the rich mixture formed by the second injection was very stable in the cylinder center from 310 °CA in Section A-A. This explains how the optimal enrichment of the spark zone can be achieved with the split-injection strategy.

5. Evaluation of engine performance

The previous section described how the BUSDIG engine was designed and evaluated by 3D CFD simulations. The key designs—including the *B/S* ratio, scavenge port angles, intake plenum, opening profiles of the intake scavenge ports and exhaust valves, and injection strategy—were investigated in order to optimize the BUSDIG engine for better performance. This section describes how the 1D engine simulations were performed based on the optimal BUSDIG designs. Different techniques—including a higher compression ratio (CR), a VVA system, water injection, diluted combustion with exhaust gas recirculation (EGR), and lean combustion—were applied in 1D engine simulations in order to identify their potential to improve the engine performance of the two-stroke BUSDIG engine. (Details of the 1D models were provided in Section 3.2.) During the simulations, the combustion duration and combustion phasing were optimized within the Wiebe model at each operating point. The EVO, which showed significant impact on the scavenging performance (as detailed in Section 4.4), was also optimized at each operating point. The opening duration of the intake scavenge ports was fixed at 100 °CA.

As shown in Fig. 26, the increase of the engine CR from 10 to 16 significantly improved the engine efficiency, from 37.27% to 40.62%. The ED was also found to be effective in improving engine efficiency due to the improved scavenging performance, as detailed in Section 4.4 and Ref. [13]. The introduction of water injection was shown to effectively suppress the knocking combustion and significantly increase the engine efficiency from 40.62% to

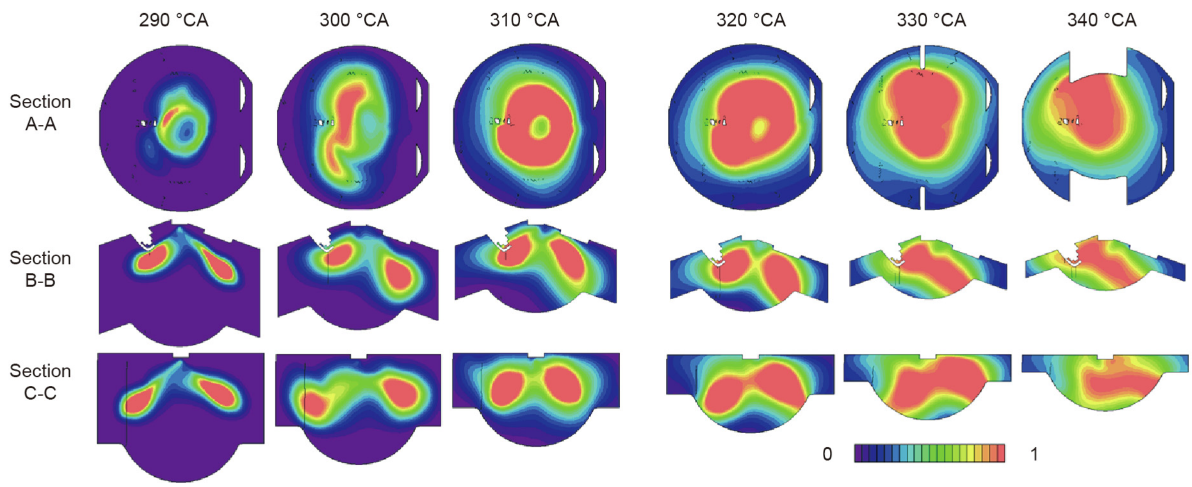

Fig. 25. Distributions of fuel/air equivalence ratio with split injection. Split ratio = 0.5, SOI = 280/300 °CA. Section A-A: horizontal plane crossing spark plug gap; Section B-B: vertical plane crossing spark plug gap and cylinder axis; Section C–C: vertical plane crossing cylinder axis and vertical to Section B-B. Reproduced from Ref. [18] with permission of Institution of Mechanical Engineers, © 2018.

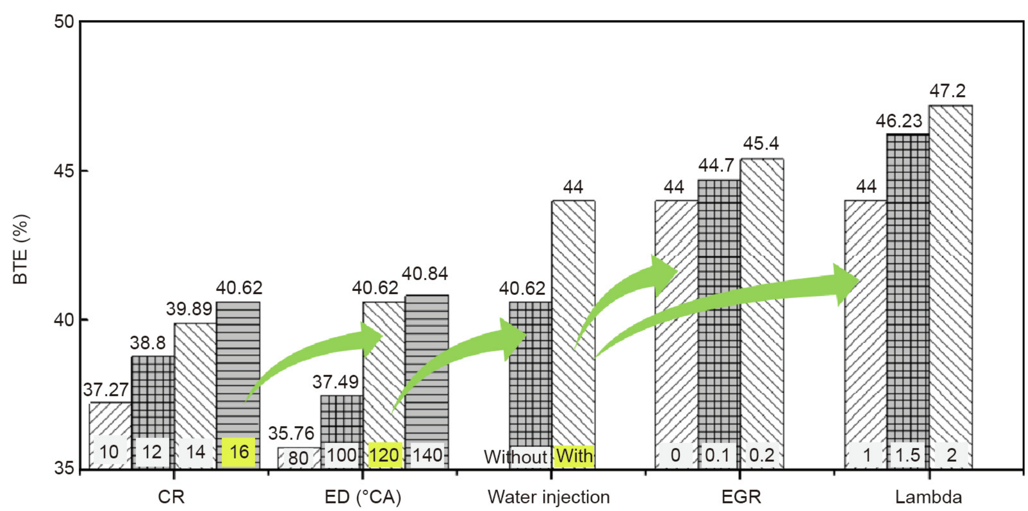

Fig. 26. Brake thermal efficiency (BTE) of the BUSDIG engine with different techniques. BTE of 44% with water injection technique was achieved at 1600 $r\cdot min^{-1}$, 1300 kPa BMEP, and 213 N·m brake torque; BTE of 45.4% with EGR technique achieved was at 1600 $r\cdot min^{-1}$, 1200 kPa BMEP, and 190 N·m brake torque; BTE of 47.2% with lambda technique was achieved at 1600 $r\cdot min^{-1}$, 1100 kPa BMEP, and 180 N·m brake torque.

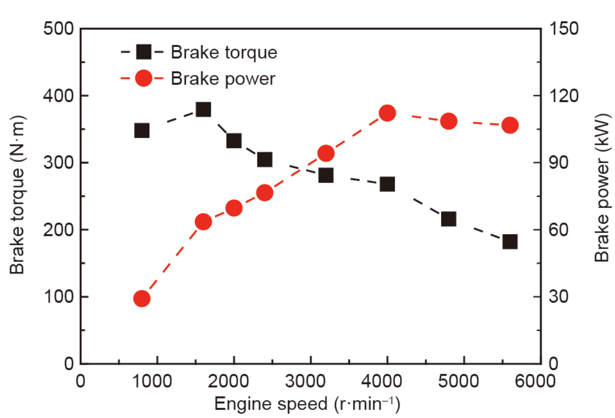

Fig. 27. Brake torque and brake power of the 1.0 L BUSDIG engine (Lambda 1 with water injection).

44%. Application of diluted combustion with 20% EGR further increased the engine efficiency to 45.4%. Alternatively, the application of ultra-lean combustion at lambda = 2 significantly increased the peak engine efficiency to 47.2%.

Fig. 27 shows the brake torque and power curves of the 1.0 L BUSDIG engine. The stoichiometric mixture was applied with water injection to suppress the knocking combustion. As shown in Fig. 27, the low-speed performance of the two-stroke BUSDIG engine was very promising, with a peak toque of 379 N·m at 1600 $r\cdot min^{-1}$. Regarding the engine power performance, it was noted that a peak brake power density of around 112 $kW\cdot L^{-1}$ could be achieved at 4000 $r\cdot min^{-1}$.

6. Conclusions

A novel two-stroke BUSDIG engine was proposed in this study to improve engine power performance and reduce fuel consumption. This paper discussed the design and optimization of the key engine components and parameters and summarized the key findings in order to highlight the progress of the development of the proposed two-stroke BUSDIG engine. The key findings can be summarized as follows:

(1) A *B/S* ratio of 0.8 with a bore of 80 mm and stroke of 100 mm was found to achieve a higher CE and TE with moderate in-cylinder flow motions for the subsequent fuel/air mixing process.

(2) Regarding the scavenge port angles, an AIA of 90° was found to be preferable in order to achieve a better scavenging performance, and a SOA of 20° was found to be optimal to produce sufficient in-cylinder flow motions and higher CE.

(3) Regarding the intake plenum design, a higher ratio of inlet area to scavenge port area ($r_{I/S}$) was found to produce a better scavenging performance with sufficient flow motions. The CE can be increased significantly when the ratio of the scavenge chamber volume to engine displacement ($r_{S/C}$) increases to 1.76. The vertical placement of the inlet pipe relative to the exhaust pipes can be used to effectively enhance the in-cylinder tumble and cross-tumble flows. A minimum scavenge port length of 10 mm was required to produce sufficient in-cylinder flow motions for subsequent fuel/air mixing in the BUSDIG engine.

(4) The opening profiles of the scavenging ports and exhaust valves were found to have a significant impact on the scavenging process in the two-stroke BUSDIG engine. A larger Δ_{open} can be used to improve the SE. The optimal scavenging performance can be achieved when the PB is just avoided by adjusting Δ_{close} and $\Delta_{overlap}$. It was also found that a low exhaust valve lift can be applied to completely avoid short-circuiting in the BUSDIG engine, and the EVO timing can be used to effectively control the scavenging performance.

(5) The engine simulations with the calibrated Reitz–Diwakar breakup model showed that the split-injection strategy with later injection timing (300/320 °CA) can be used to produce a stable rich mixture (fuel/air equivalence ratio ≈ 1.1) around the spark plug with an overall lean mixture (lambda ≈ 1.7).

(6) The application of a higher CR, a longer ED, water injection, and diluted and lean combustion were found to be effective in improving the brake thermal efficiency of the two-stroke BUSDIG engine. A peak brake thermal efficiency of 47.2% was achieved with lean combustion at lambda = 2. A peak brake toque of 379 N·m and a peak brake power density of 112 $kW\cdot L^{-1}$ were achieved at 1600 and 4000 $r\cdot min^{-1}$, respectively, in the BUSDIG engine with the stoichiometric condition.

Acknowledgements

The authors gratefully acknowledge financial support from the Engineering and Physical Sciences Research Council (EPSRC)[†].

Compliance with ethics guidelines

Xinyan Wang and Hua Zhao declare that they have no conflict of interest or financial conflicts to disclose.

References

[1] Fraser N, Blaxill H, Lumsden G, Bassett M. Challenges for increased efficiency through gasoline engine downsizing. SAE Int J Engines 2009;2(1):991–1008.
[2] Dingle S, Cairns A, Zhao H, Williams J, Williams O, Ali R. Lubricant induced pre-ignition in an optical SI engine. SAE Technical Paper 2014:2014-01-1222.
[3] Benajes J, Novella R, De Lima D, Tribotte P. Investigation on multiple injection strategies for gasoline PPC operation in a newly designed 2-stroke HSDI compression ignition engine. SAE Int J Engines 2015;8(2):758–74.
[4] Dalla Nora M, Lanzanova T, Zhang Y, Zhao H. Engine downsizing through two-stroke operation in a four-valve GDI engine. SAE Technical Paper 2016:2016-01-0674.
[5] Mattarelli E, Rinaldini CA. Two-stroke gasoline engines for small-medium passenger cars. SAE Technical Paper 2015:2015-01-1284.
[6] Zhang Y, Nora MD, Zhao H. Comparison of performance, efficiency and emissions between gasoline and E85 in a two-stroke poppet valve engine with lean boost CAI operation. SAE Technical Paper 2015:2015-01-0827.
[7] Nishida K, Sakuyama H, Kimijima T. Improvement of fuel economy using a new concept of two-stroke gasoline engine applying stratified-charge auto-ignition. SAE Technical Paper 2009:2009-28-0009.
[8] Johnson J, Den Braven KR. Comparison of homogeneous, stratified and high-squish stratified combustion in a direct-injected two-stroke engine. SAE Technical Paper 2008:2008-32-0030.
[9] Wang X, Zhao H, Xie H. Effect of dilution strategies and direct injection ratios on stratified flame ignition (SFI) hybrid combustion in a PFI/DI gasoline engine. Appl Energy 2016;165:801–14.
[10] Wang X, Zhao H, Xie H. Effect of piston shapes and fuel injection strategies on stoichiometric stratified flame ignition (SFI) hybrid combustion in a PFI/DI gasoline engine by numerical simulations. Energy Convers Manage 2015;98:387–400.
[11] Wang X, Ma J, Zhao H. Analysis of the effect of bore/stroke ratio and scavenge port angles on the scavenging process in a two-stroke boosted uniflow scavenged direct injection gasoline engine. Proc Inst Mech Eng, D J Automob Eng 2018;232(13):1799–814.
[12] Wang X, Ma J, Zhao H. Evaluations of scavenge port designs for a boosted uniflow scavenged direct injection gasoline (BUSDIG) engine by 3D CFD Simulations. SAE Technical Paper 2016:2016-01-1049.
[13] Wang X, Ma J, Zhao H. Analysis of scavenge port designs and exhaust valve profiles on the in-cylinder flow and scavenging performance in a two-stroke boosted uniflow scavenged direct injection gasoline engine. Int J Engine Res 2018;19(5):509–27.
[14] Ma J, Zhao H. The modeling and design of a boosted uniflow scavenged direct injection gasoline (BUSDIG) engine. SAE Technical Paper 2015:2015-01-1970.
[15] Wang X, Ma J, Zhao H. Analysis of the impact of exhaust valve profile on the scavenging and combustion process in a two-stroke boosted uniflow scavenged gasoline (BUSDIG) engine. In: Proceedings of the IMechE Internal Combustion Engines Conference 2017 Dec 6–7; Birmingham, UK; 2017.
[16] Wang X, Ma J, Zhao H. Analysis of the effect of intake plenum design on the scavenging process in a two-stroke boosted uniflow scavenged direct injection gasoline (BUSDIG) engine. SAE Technical Paper 2017:2017-01-1031.
[17] Wang X, Zhao H. Numerical simulation of the gasoline spray with an outward-opening piezoelectric injector: a comparative study of different breakup models. SAE Technical Paper 2018:2018-01-0272.
[18] Wang X, Ma J, Zhao H. Analysis of mixture formation process in a two-stroke boosted uniflow scavenged direct injection gasoline engine. Int J Engine Res 2018;19(9):927–40.
[19] Sigurdsson E, Ingvorsen KM, Jensen MV, Mayer S, Matlok S, Walther JH. Numerical analysis of the scavenge flow and convective heat transfer in large two-stroke marine diesel engines. Appl Energy 2014;123:37–46.
[20] Andersen FH, Mayer S. CFD analysis of the scavenging process in marine twostroke diesel engines. In: Proceedings of the ASME 2014 Internal Combustion Engine Division Fall Technical Conference; 2014: Oct 19–22; Columbus, IN, USA; 2014.
[21] Mattarelli E, Rinaldini CA, Baldini P. Modeling and Experimental Investigation of a 2-stroke GDI engine for range extender applications. SAE Technical Paper 2014:2014-01-1672.
[22] Hori H. Scavenging flow optimization of two-stroke diesel engine by use of CFD. SAE Technical Paper 2000:2000-01-0903.
[23] Laget O, Ternel C, Thiriot J, Charmasson S, Tribotté P, Vidal F. Preliminary design of a two-stroke uniflow diesel engine for passenger car. SAE Int J Engines 2013;6(1):596–613.
[24] Lee C, Zhao H, Ma T. A simple and efficient mild air hybrid engine concept and its performance analysis. Proc Inst Mech Eng, D J Automob Eng 2013;227(1):120–36.
[25] Borghi M, Mattarelli E, Muscoloni J, Rinaldini CA, Savioli T, Zardin B. Design and experimental development of a compact and efficient range extender engine. Appl Energy 2017;202:507–26.
[26] Turner J, Blundell DW, Pearson RJ, Patel R, Larkman DB, Burke P, et al. Project omnivore: a variable compression ratio atac 2-stroke engine for ultra-wide-range HCCI operation on a variety of fuels. SAE Int J Engines 2010;3(1):938–55.
[27] Blundell DW, Turner J, Pearson R, Patel R, Young J. The omnivore wide-range auto-ignition engine: results to date using 98RON unleaded gasoline and E85 fuels. SAE Technical Paper 2010:2010-01-0846.
[28] CD-adapco. Methodology, STAR-CD version 4.14. Melville: CD-adapco; 2010.
[29] Han Z, Reitz RD. Turbulence modeling of internal combustion engines using RNG κ-ε Models. Combust Sci Technol 1995;106(4–6):267–95.
[30] Jones WP. Prediction methods for turbulent flames. In: Kollmann W, Kollmann W, editors. Prediction methods for turbulent flow. Washington: Hemisphere; 1980. p. 1–45.
[31] Angelberger C, Poinsot T, Delhay B. Improving near-wall combustion and wall heat transfer modeling in SI engine computations. SAE Technical Paper 1997:972881.
[32] Lefebvre A. Atomization and sprays. Cleveland: CRC Press; 1988.
[33] Reitz RD, Diwakar R. Effect of drop breakup on fuel sprays. SAE Technical Paper 1986:860469.
[34] Bai C, Gosman AD. Development of methodology for spray impingement simulation. SAE Technical Paper 1995:950283.
[35] Issa RI. Solution of the implicit discretised fluid flow equations by operator-splitting. J Comput Phys 1986;62(1):40–65.
[36] Douaud AM, Eyzat P. Four-octane-number method for predicting the anti-knock behavior of fuels and engines. SAE Technical Paper 1978:780080.
[37] Chen SK, Flynn PF. Development of a single cylinder compression ignition research engine. SAE Technical Paper 1965:650733.

[†] The data for this research can be accessed from the Brunel University London data archive, figshare at https://doi.org/10.17633/rd.brunel.7862522.v1.

[38] Ma J. Numerical and experimental study of a boosted uniflow 2-stroke engine [dissertation]. London: Brunel University London; 2014.
[39] Williams AM, Baker AT, Garner CP, Vijayakumar R. Turbo-discharging turbocharged internal combustion engines. Proc Inst Mech Eng, D J Automob Eng 2013;227(1):52–65.
[40] Regner G, Herold RE, Wahl MH, Dion E,Redon F, Johnson D. The achates power opposed-piston two-stroke engine: performance and emissions results in a medium-duty application. SAE technical paper 2011:2011-01-2221.
[41] Zhang Y, Zhao H. Measurement of short-circuiting and its effect on the controlled autoignition or homogeneous charge compression ignition combustion in a two-stroke poppet valve engine. Proc Inst Mech Eng, D J Automob Eng 2012;226(8):1110–8.
[42] Hult J, Matlok S, Mayer S. Particle image velocimetry measurements of swirl and scavenging in a large marine two-stroke diesel engine. SAE Technical Paper 2014:2014-01-1173.
[43] Ingvorsen KM, Meyer KE, Walther JH, Mayer S. Turbulent swirling flow in a dynamic model of a uniflow-scavenged two-stroke engine. Exp Fluids 2014;55 (6):1748.
[44] Han Z, Fan L, Reitz RD. Multidimensional modeling of spray atomization and air-fuel mixing in a direct-injection spark-ignition engine. SAE Technical Paper 1997:970884.
[45] Ruhland H, Lorenz T, Dunstheimer J, Breuer A, Khosravi M. A study on charge motion requirements for a class-leading GTDI engine. SAE Technical Paper 2017:2017-24-0065.
[46] Miles PC, Andersson Ö. A review of design considerations for light-duty diesel combustion systems. Int J Engine Res 2016;17(1):6–15.
[47] Altin I, Sezer I, Bilgin A. Effects of the stroke/bore ratio on the performance parameters of a dual-spark-ignition (DSI) engine. Energy Fuels 2009;23 (4):1825–31.
[48] Lee C, Goel S, Babajimopoulos A. The effects of stroke-to-bore ratio on HCCI combustion. SAE Technical Paper 2010:2010-01-0842.
[49] Yang X, Okajima A, Takamoto Y, Obokata T. Numerical study of scavenging flow in poppet-valved two-stroke engines. SAE Technical Paper 1999:1999-01-1250.
[50] Thornhill D, Douglas R, Kenny R, Fitzsimons B. An experimental investigation into the effect of bore/stroke ratio on a simple two-stroke cycle engine. SAE Technical Paper 1999:1999-01-3342.
[51] Kee RJ, Blair GP, Douglas R. Comparison of performance characteristics of loop and cross scavenged two-stroke engines. SAE Technical Paper 1990:901666.
[52] Zhu Y, Savonen C, Johnson NL, Amsden AA. Three-dimensional computations of the scavenging process in an opposed-piston engine. SAE Technical Paper 1994:941899.
[53] Wang X, Xie H, Zhao H. Computational study of the influence of in-cylinder flow on spark ignition–controlled auto-ignition hybrid combustion in a gasoline engine. Int J Engine Res 2015;16(6):795–809.
[54] Ingvorsen KM, Meyer KE, Walther JH, Mayer S. Phase-locked stereoscopic PIV measurements of the turbulent swirling flow in a dynamic model of a uniflowscavenged two-stroke engine cylinder. In: Proceedings of the 10th International Symposium On Particle Image Velocimetry; 2013 Jul 1–3; Delft, The Netherlands; 2013.
[55] Haider S, Schnipper T, Obeidat A, Meyer KE, Okulov VL, Mayer S, et al. PIV study of the effect of piston position on the in-cylinder swirling flow during the scavenging process in large two-stroke marine diesel engines. J Mar Sci Technol 2013;18(1):133–43.
[56] Tamamidis P. Assanis DN. Optimization of inlet port design in a uniflow-scavenged engine using a 3-D turbulent flow code. SAE Technical Paper 1993:931181.
[57] Abis A, Winkler F, Schwab C, Kirchberger R, Eichlseder H. An innovative two-stroke twin-cylinder engine layout for range extending application. SAE Technical Paper 2013:2013-32-9133.
[58] Vashishtha A, Rathinam B. Study of intake ports design for ultra low cost (ULC) gasoline engine using STAR-CD. SAE Technical Paper 2012:2012-01-0407.
[59] Blair GP. Design and simulation of two-stroke engines. Warrendale: Society of Automotive Engineers; 1996.
[60] Zhang Y, Zhao H, Ojapah M, Cairns A. CAI combustion of gasoline and its mixture with ethanol in a 2-stroke poppet valve DI gasoline engine. Fuel 2013;109:661–8.
[61] Zhang Y. 2-stroke CAI combustion operation in a GDI engine with poppet valves. SAE Technical Paper 2012:2012-01-1118.
[62] Ravi MR, Marathe AG. Effect of port sizes and timings on the scavenging characteristics of a uniflow scavenged engine. SAE Technical Paper 1992:920782.
[63] Carlucci AP, Ficarella A, Trullo G. Performance optimization of a two-stroke supercharged diesel engine for aircraft propulsion. Energy Convers Manage 2016;122:279–89.
[64] Persson H, Sjoholm J, Kristensson E, Johansson B, Richter M, Alden M. Study of fuel stratification on spark assisted compression ignition (SACI) combustion with ethanol using high speed fuel PLIF. SAE Technical Paper 2008:2008-01-2401.
[65] Williams B, Ewart P, Wang X, Stone R, Ma H, Walmsley H, et al. Quantitative planar laser-induced fluorescence imaging of multi-component fuel/air mixing in a firing gasoline-direct-injection engine: effects of residual exhaust gas on quantitative PLIF. Combust Flame 2010;157(10):1866–78.
[66] Middleton RJ, Martz JB, Lavoie GA, Babajimopoulos A, Assanis DN. A computational study and correlation of premixed isooctane air laminar reaction fronts diluted with EGR. Combust Flame 2012;159(10): 3146–57.
[67] Benajes J, García A, Domenech V, Durrett R. An investigation of partially premixed compression ignition combustion using gasoline and spark assistance. Appl Therm Eng 2013;52(2):468–77.
[68] Dahl D, Andersson M, Berntsson A. Denbratt I. Reducing pressure fluctuations at high loads by means of charge stratification in HCCI combustion with negative valve overlap. SAE Technical Paper 2009:2009-01-1785.
[69] Iyer CO, Han Z, Yi J. CFD modeling of a vortex induced stratification combustion (VISC) system. SAE Technical Paper 2004:2004-01-0550.
[70] Oh H, Bae C. Effects of the injection timing on spray and combustion characteristics in a spray-guided DISI engine under lean-stratified operation. Fuel 2013;107:225–35.
[71] Costa M, Sorge U, Allocca L. Increasing energy efficiency of a gasoline direct injection engine through optimal synchronization of single or double injection strategies. Energy Convers Manage 2012;60:77–86.
[72] Ikoma T, Abe S, Sonoda Y, Suzuki H. Development of V-6 3.5-liter engine adopting new direct injection system. SAE Technical Paper 2006:2006-01-1259.
[73] Drake MC, Haworth DC. Advanced gasoline engine development using optical diagnostics and numerical modeling. Proc Combust Inst 2007;31 (1):99–124.